A compact dosimetric system for MOSFETs based on passive NFC tag and smartphone

M.A. Carvajal[1,*], P. Escobedo[1], M. Jiménez-Melguizo [2], M.S. Martínez-García [3], F. Martínez-Martí[4], A. Martínez-Olmos[1], A.J. Palma[1]

Address:

[1] ECsens, CITIC-UGR, Departamento de Electrónica y Tecnología de Computadores. Universidad de Granada, E-18071 Granada, Spain.

[2] Unidad de Radiofísica, Hospital Universitario San Cecilio, Granada, Spain.

3 Dpto. Tecnología Electrónica y de las Comunicaciones, Escuela Politécnica Superior, Universidad Autónoma de Madrid, E-28049 Madrid, Spain.

[4] Life Supporting Technologies, Universidad Politécnica de Madrid, E.T.S.I. Telecomunicación - D.108, Avda. Complutense, 30 - 28040 Madrid - Spain

mail: carvajal@ugr.es

ABSTRACT

In this work we describe and evaluate a dosimetric system based on an NFC (Near Field Communication) tag and a smartphone that uses commercial MOSFETs as radiation sensors. The tag is designed with commercial integrated circuits and the smartphone is the power source of the tag configured as a readout unit, user interface and storage unit. The NFC tag is supplied wirelessly by the smartphone via NFC, using a home-made structure to align the tag coil and smartphone coil in order to achieve a good inductive coupling. In this case, the commercial DMOS transistor ZVP3306 is used as dosimeter in unbiased mode, connected to the tag before and after each irradiation session to perform the sensor reading. An evaluation of the dosimetric system has been carried out irradiating three transistors with photon beam of 6 MV up to 20 Gy. The average sensitivity found is (4.75 ± 0.15) mV/Gy, which is in good agreement with the results found with our previously developed dosimetric system. Therefore, this miniaturised dosimetric system can be considered as a promising and low cost electronic architecture to be used for dosimetry control in radio-therapy treatments.

Keywords: NFC passive tag, MOSFET dosimeter, unbiased mode, smartphone.

1. Introduction

In-vivo dosimetry is a complementary technique to improve the quality of radiotherapy treatments. The energy provided to the tumour must be high enough to destroy it, but the damage to surrounding tissues must be minimized. The use of small sensor devices is highly advisable in order to reduce the distortion of the irradiation delivered to the patient. Therefore, pMOSFET (p channel MOSFET) dosimeters are suitable for in-vivo dosimetry. In addition, pMOSFETs present good linearity, immediate readout and the calibration can be carried out easily [1–4]. Thanks to these benefits, the use of pMOSFET dosimeters is becoming more popular in radiotherapy treatments. In fact, there are several commercial dosimetric systems based on pMOSFETs [5–7] and some research groups have developed their own systems [8,9]. When a MOS transistor is exposed to radiation, electron-holes pairs are produced in the whole device. However, only in the zones where there is an electric field the electron and the hole are separated. If all terminals are short-circuited, there is electric field only in the gate-oxide and in the SiO_2-Si interface of the structure. Thus, the main active area is the gate-oxide region and, to a lesser extent, the SiO_2-Si interface [10,11]. To improve the sensitivity, transistors with a thick oxide, grown with special technological processes, were developed. The result is pMOSFETs that are specially manufactured for radiation detection, known as RADFETs (RADiation FETs) [12–14]. However, for typical radiotherapy doses, commercial transistors can be used as dosimeters instead of RADFETs if an adequate signal amplification and filtering are carried out [15–17]. In such cases, the cost of patient monitoring would be considerably reduced. The cost of the reader unit is not negligible in a dosimetry system. Therefore, if the reader unit was replaced by a low-cost device, the final cost of a dosimetric system could be very affordable.

The use of a smartphone as a reader for different sensors would results in considerable cost savings and facilitate the access to market [18]. Furthermore, if the communication between the smartphone and the sensor is done via some radiofrequency protocol such as Near Field Communication protocol (NFC) [19], the contact between the smartphone and the sensor tag is not necessary. Several research groups have developed NFC tags with sensing capabilities [20–22]. Depending on the power consumption requirements, the NFC tag can be developed without battery or any other power source, thus reducing the overall cost [23,24]. In such cases, an NFC-enabled smartphone can wirelessly energize the NFC tag through inductive coupling and transfer data by means of signal modulation [25–27]. The energy harvested from the RF field can also be used to supply some external circuitry, for example a microcontroller [28], a DC/DC converter [29] or analog circuitry [30]. However, a perfect tuning and alignment with a high quality factor antenna is required.

In this case, the power consumption for dose measurements with MOSFETs is usually low [3,8,9] In fact, Sicel Technologies (Morrisville, North Carolina, USA) developed an implantable MOS dosimeter consisting of an RFID tag that works in low frequency band (LF) [31–33]. This system uses an Application Specific Integrated Circuit (ASIC) RFID chip

with a ferrite coil. Therefore, to measure the dose by means of the NFC protocol is expected to be possible.

In this work, we present the development and characterization of a dose reader system for commercial pMOSFETs composed of a smartphone and an NFC tag. The sensor module is connected to the NFC tag configured as a reader unit. An Android^{TM} application has been designed to use an NFC-enabled smartphone for wirelessly powering the system up and reading the dose measurements. The hardware included in the system is developed using commercial integrated circuits, including the radiation sensor. No ASIC circuits are needed, thus the cost will be considerably reduced. In addition, a whole reader unit is not necessary to carry out dose measurements, only the NFC tag and a smartphone. Moreover, the system performance has been compared with our previously developed reader unit [9] showing very good agreement.

2. Experimental

Numerical simulations for tag antenna optimization were carried out with Advanced Design Simulator (ADS, Keysight Technologies, Santa Clara, California, USA). Antenna and reader tag were fabricated on 1.5 mm thick FR4 substrate using a mechanical milling machine model ProtoMat S100 (LPKF Laser & Electronics AG, Garbsen, Germany). The FR4 substrate has a relative permittivity of ε_r=4.6 and a loss tangent of tanδ=0.015. Metallization layer is 35 μm thick copper with a conductivity of σ=4.6×107 S⁄m.

For electrical characterization of the tag antenna an impedance analyser was used, the Agilent 4294A (Keysight Technologies, Santa Clara, California, USA). For thermal measurements, four devices were introduced into a climate chamber model VCL4006 (Vötoshch Industryetedhnik, Germany) while the electrical parameters were registered with a multimeter Agilent 34410A (Agilent, USA). For the app, Android Studio 2.3.1 was used as the integrated development environment (IDE). The application was designed and tested against API level 22 (Android 5.1), although the lowest API level compatible is API level 16 (Android 4.1). The smartphone used in this work as the NFC reader was the Sony Xperia S.

A different set of three sensor modules based on the commercial pMOSFET ZVP3306 (Zetex Diode, USA) were irradiated with a linear accelerator Siemens Artiste (Siemens AG, Germany). A total of 20 Gy were provided in a series of five sessions of 4 Gy each, with a field of 10×10 cm^2 with photon beams of 6 MV. The sensors were placed at the isocenter of the irradiation source. In order to achieve the electronic equilibrium, a 1.5 cm build-up layer of solid water was placed over the transistors. To control LINAC stability and to verify dose measurements, a PTW23332 ionization chamber (Radia-tion Products Design, Inc.; Albertville, France) was placed under the sensor modules for every irradiation session.

To evaluate the response of the NFC reader unit and compare it with other instrumentation, our previous reader unit [17,34] was used as reference system. This dosimetric reader unit can measure the source voltage shift with a resolution of 0.25 mV. The increment of the source voltage of the transistor was measured at constant drain current, which is the simplest method to evaluate the threshold voltage shift [3,10,11].

3. NFC tag and sensor module architectures

The NFC tag consists of the following functional blocks: RFID chip and antenna, a charge pump to increase the supply voltage, a current source, conditioning electronic and a socket to connect the sensor module. The block diagram of the NFC tag is displayed in Figure 1. The different parts of the NFC tag will be described in following subsections. As can be seen from Figure 2, the developed tag operates without battery, only with the energy harvested from the electromagnetic field coming from the smartphone NFC link.

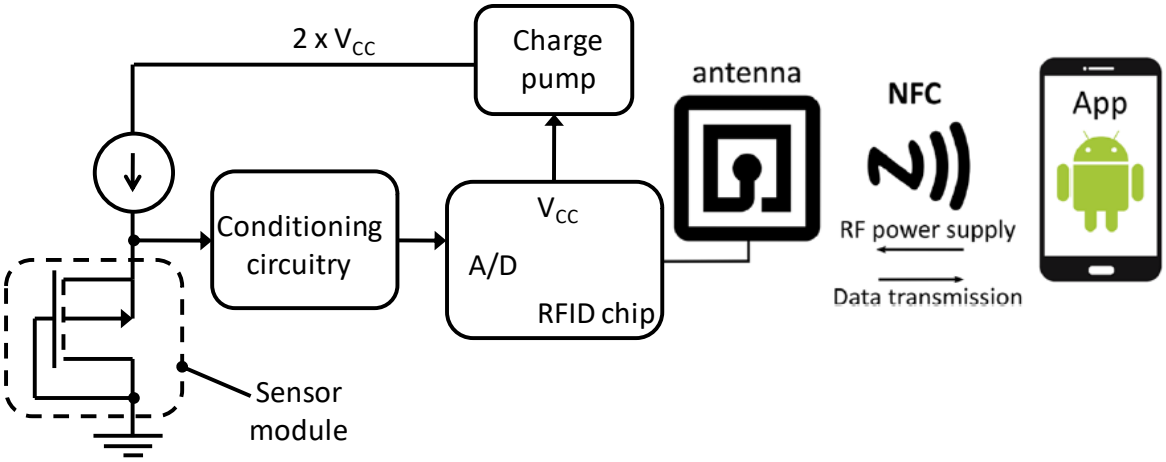

Figure 1. NFC tag and sensor module block diagram[1].

[1] The Android robot is reproduced or modified from work created and shared by Google and used according to terms described in the Creative Commons 3.0 Attribution License.

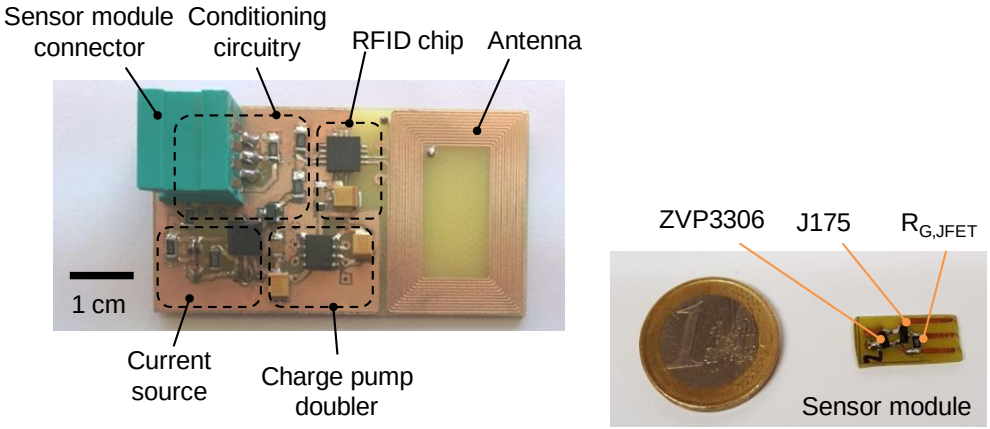

Figure 2. NFC tag with the functional blocks highlighted (left) and sensor module (right).

3.1. RFID chip and antenna

The NFC chip SL13A (AMS AG, Unterpremstätten, Austria) along with a custom-designed RFID antenna is used for energy harvesting, communication and sensor acquisition purposes [35]. This chip operates in HF band and it has a sensor front end (SFE) that is able to measure voltage, current, resistance and capacitance. In this work, the SFE is used as a single voltage input for the built-in analog-to-digital converter (ADC) of the chip. The ADC input signal must lie between 300 and 600 mV. Therefore, conditioning circuitry is needed to measure the pMOSFET source voltage. In addition, energy harvesting capabilities of the chosen NFC chip enable the development of battery-free designs. The integrated circuit can provide a regulated voltage of 3.2 V with an output current up to 4 mA if the external RF electromagnetic field from the RFID reader is adequate. Therefore, this RFID chip is able to provide up to 12.8 mW without battery, which is enough to supply some additional circuitry.

The antenna consists of a PCB custom-designed planar coil and the internal capacitor of the SL13A (see Figure 2). The RFID chip communicates with the smartphone through the antenna and, in addition, the energy is harvested through the antenna and supplies the tag. The chosen NFC chip integrates an internal tuning capacitor with a value of 25 pF at the frequency of interest, 13.56 MHz. Thus, a simple coil with a value of 5.5 µH is required to obtain a parallel LC circuit resonant at 13.56 MHz. The designed antenna coil has 12 turns and dimensions of 30 mm × 20 mm. The width of the conductor is 200 µm and the interspacing between the lines is 250 µm. The final number of turns and dimensions were obtained after optimization process with numerical simulations.

3.2. Signal and power conditioning

The measurement of the source voltage shifts at constant current is probably the easiest way to measure the threshold voltage shifts of pMOSFET as radiation sensor. To do so, a current source must be included in the tag as well as a buffer to avoid that the conditioning circuit loads the current source. Thus, the minimal analog circuitry needed to carry out dose measurements is a current source and a buffer with conditioning circuitry. The integrated circuit LM334 of Texas Instruments (Dallas, Texas, USA) has been used to implement the current source. In the present work, we have implemented the circuit topology recommended by the manufacturer of the LM334 to reduce the thermal drift of the output current by using two resistors and diode.

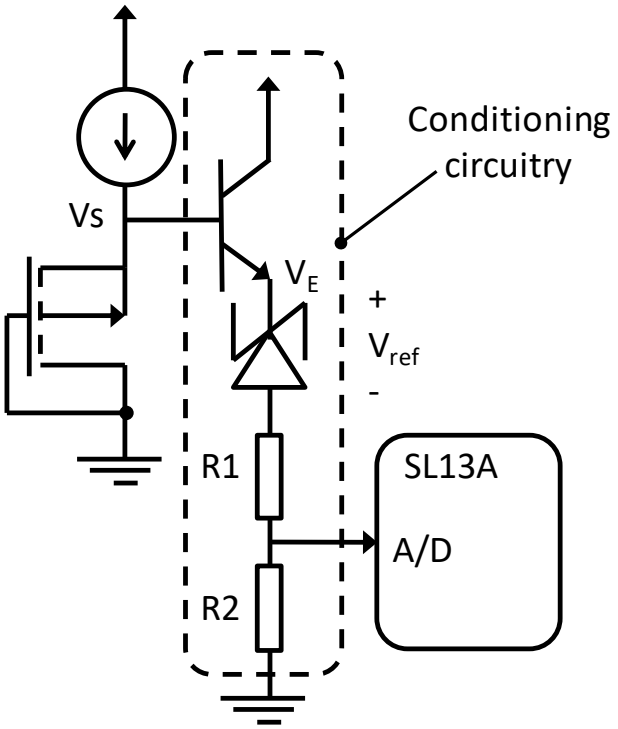

Figure 3. Buffer, voltage shift and voltage divider circuit schema of the tag reader.

The buffer consists of a general propose bipolar transistor model BC848 (Infineon AG, Germany), which avoids the subtraction of drain current by the voltage divider and ADC of the SL13A, as shown in Figure 3. The collector current depends on the value of source voltage, V_S, and it must be set for each transistor model and drain current selected, as it is described in following sections for the transistor ZVP3306. The output of the conditioning circuitry must lie between 300 and 600 mV because this is the input voltage range of the ADC. Thus, a voltage divider is required and implemented with R1 and R2 resistors. Moreover, a voltage shift of a reference voltage, V_{ref}, has been included to reduce the voltage

before the ADC, as Figure 3 shows. According to the conditioning circuit depicted in Figure 4, the input voltage of the ADC is given by equation (1):

$$V_{in}^{ADC} = \frac{R_2}{R_1+R_2}\left(V_S - V_{BE} - V_{ref}\right) \quad (1)$$

The selected V_{ref} was the LM385-1.2 of Texas Instruments (USA) that provides a stable voltage of 1.23 V with a typical thermal dependence of 20 ppm/ºC. The main restriction is that the reverse current must be between 0.01 and 20 mA. Taking into account that the voltage source of the ZVP3306 was around 2.6 V at the chosen bias current, the resistors R1 and R2 were selected as 15 kΩ to ensure a reserve current in the LM385 of 0.03 mA, which is in the correct range of this reference voltage.

The power harvested by the antenna, after being rectified and regulated by the RFID chip, is used to supply the switch capacitor voltage doubler based on ADM660 integrated circuit (Analog Devices, USA). This chip was chosen due to its low quiescent current, 600 µA, and the easy doubler configuration in which only two external capacitors are required. In this way, the regulated voltage of 3.2 V is increased up to 6.4 V in order to increase the maximum drain-source voltage. Assuming a DC/DC efficiency of 80 %, and considering the quiescent current of the ADM660, the total power that must be provided by the SL13A is around 4 mW. This power can be supplied by the SL13A if the inductive coupling between the coil of the smartphone and the coil of the tag is appropriate.

3.3. Sensor module

The sensor module is based on the general purpose DMOS ZVP3306 and it was previously evaluated as radiation sensor with our reader unit [34]. This transistor was selected due to its ionizing response, low cost (below 0.3 €) and because it is commercially available. In addition, the DMOS structure is very common in current MOSFETs, therefore another study of this kind of MOSFET would be interesting in order to study their response to ionizing radiation. Basically, the sensor module consists of the pMOS transistors as radiation sensor and a JFET that prevents the damage due to electrostatic discharge during the storage and irradiation period, as Figure 4 shows. The configuration is similar to the sensor module presented in previous works [9], but with minor modifications. The JFET used in our previous work was an N-channel transistor, which connects the source and drain terminals of the pMOS. This JFET must be cut off during the reading process by biasing the JFET gate with a negative voltage, so the connection between the source and drain of the pMOS is interrupted and the current flows through the pMOS transistor [9]. However, in the present work a negative voltage is not available in the NFC tag, so N-channel JFET cannot be used. Therefore, a P-channel JFET must be used despite its higher ON resistance. The J175 from NXP Semiconductors (Eindhoven, Netherlands) was selected. This device presents a typical

ON resistor of 125 Ω and a gate-source cut-off voltage of 3 to 6 V. In our case, the gate was connected directly to the power supply voltage, which was enough to cut off the JFET.

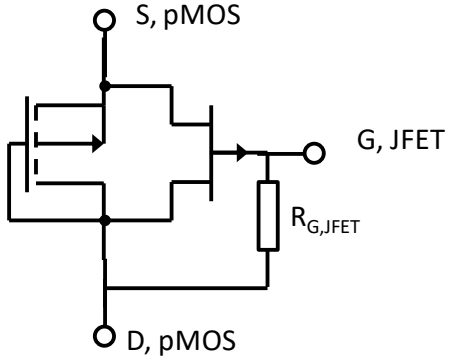

Figure 4. Sensor module schematic.

3.4. Current bias selection for read-out

The pMOSFET drain and BJT collector currents (see Figure 3) were selected both to bias the device properly for reading out and to reduce the thermal coefficient of the emitter voltage. The thermal behaviour assumed in the present work is a linear model, as already assumed with good results in our previous works [34,36,37]. Therefore, the voltage increments due to temperature changes (ΔT) can be written as follows:

$$\Delta V_{in}^{ADC} = \alpha \Delta T \, , \Delta V_S = \alpha_S \Delta T, \Delta V_{BE} = \alpha_{BE} \Delta T \tag{2}$$

where α is the thermal coefficient of the ADC input voltage, α_S is the thermal coefficient of the source voltage and α_{BE} is the thermal coefficient of the base-emitter voltage. Neglecting the thermal dependence of the voltage divider and the reference voltage, the thermal coefficient of the input A/D converter voltage can be obtained from Equation (1) as follows:

$$\alpha = \frac{R_2}{R_1 + R_2} (\alpha_S - \alpha_{BE}) \tag{3}$$

If α_S and α_{BE} are very similar, the thermal dependence of the voltage input of the ADC will be minimized. According to our previous work [34], the thermal coefficient of the source voltage of the ZVP3306 in saturation region with gate and drain short-circuited and biased at a current of 220 µA was (-2.30 ± 0.12) mV/ºC. In the same work, the reverse diode was characterized as temperature sensor, obtaining a thermal coefficient of (-2.332 ± 0.013) mV/ºC for a diode current of 30 µA.

In the case of our previous reader unit, an operational amplifier instead of a bipolar transistor was used as buffer. Thus, the method described above cannot be applied to reduce the thermal dependence in dose measurements with the previous reader unit. To minimize the thermal drift in that case, the drain current selected to measure the increment of source voltage was 100 µA. At that current, the thermal coefficient was minimum for these transistors (2.04 ± 0.12) mV/ºC [34]. To sum up, the drain currents used for dose measurements are 220 µA and 100 µA for the NFC reader and our previous reader respectively, and 30 µA for the collector current of the buffer in the NFC reader.

4. Android application and readout setup

The chosen SL13A chip is compliant with the ISO15693 RFID standard and compatible with Android near-field communication (NFC-V standard). The application is based on the use of ISO15693 and cool-Log commands. These latter are EPC (Electronic Product Code) custom commands with the same structure as the standard ISO15693 commands. Figure 5 shows a screenshot of the application user interface. It consists of several text fields showing information about the tag identification number, temperature and the digital value of the external voltage read through the SFE of the chip.

Once the phone is approached to the tag, the user can start the application, which programmatically activates the NFC of the phone (see Figure 5). The system is powered up by the electromagnetic energy from the mobile NFC link, the tag is detected and the measurements are taken The ADC measurements from the external sensor interface analog input are taken within an independent thread of the application that executes during 10 seconds, reading a value of the ADC each 500 milliseconds. Each measurement is written on a file that is stored in the internal memory of the phone. After that, the NFC is automatically turned off. It is important to switch the NFC on at the beginning of the measurement and then switch it off when the measurement is concluded, because when a pMOSFET is biased an initial decay of source-voltage is produced due to activation of low state. The effect of this decay is minimized if the time during which the pMOSFET is biased before the source voltage measurement is the same in every measurement. It should be noted that the smartphone needs to be rooted first since Android API does not allow to enable or disable NFC programmatically without root access.

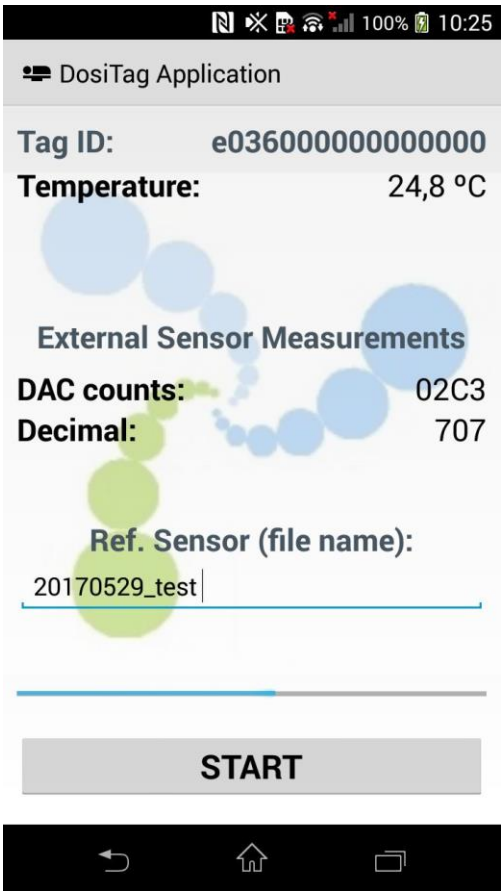

Figure 5. Screenshot of the custom designed Android application.

The alignment for identification of an NFC tag is not critical if the power consumption of the tag is low, as it happens in typical digital applications such as contactless payments. However, in tags with sensing capabilities with higher power consumption, the inductive coupling between the external NFC reader coil and the tag coil must be good enough. The distance must be as short as possible and both coils should be overlapped to optimize the energy harvested by the tag. In our case, a wood structure was handmade to ensure the adequate and repeatable inductive coupling. The tag is placed into the structure keeping the sensor socket accessible, as shown in the Figure 6.

Figure 6. Experimental setup for NFC measurements

5. Results and discussion

5.1. Electromagnetic performance

We have measured the inductance and quality factor of the PCB coil without the SL13A chip, as shown in Figure 7a. The inductance at 13.56 MHz is 5.41 µH, very close to the designed value. In addition, the quality factor achieved using a FR-4 substrate is higher than 60, enough for this type of applications, and the self-resonance frequency is much higher than 13.56 MHz, about 36 MHz in our case. Therefore, the coil can be considered valid for our requirements. Once the SL13A is attached to the PCB, the resonant circuit is completed. Thus a new frequency characterization was carried out, measuring the impedance and phase of the L||C resonant circuit. In order to fine-tune the resonant frequency, a 4.9 pF parallel capacitor has been included. As can be observed in Figure 7b, the measured resonant frequency is 13.575 MHz, which is very close to the desired working frequency of 13.56 MHz.

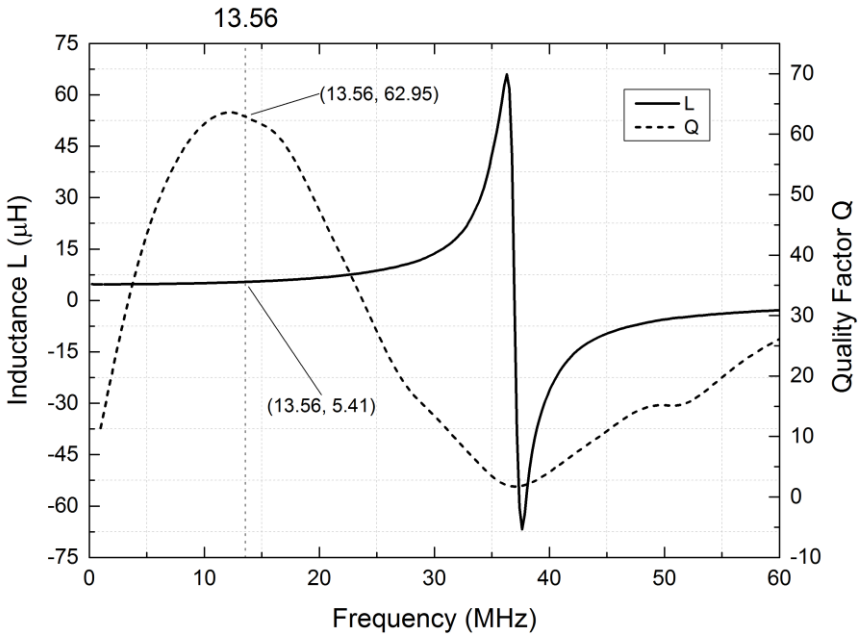

(a)

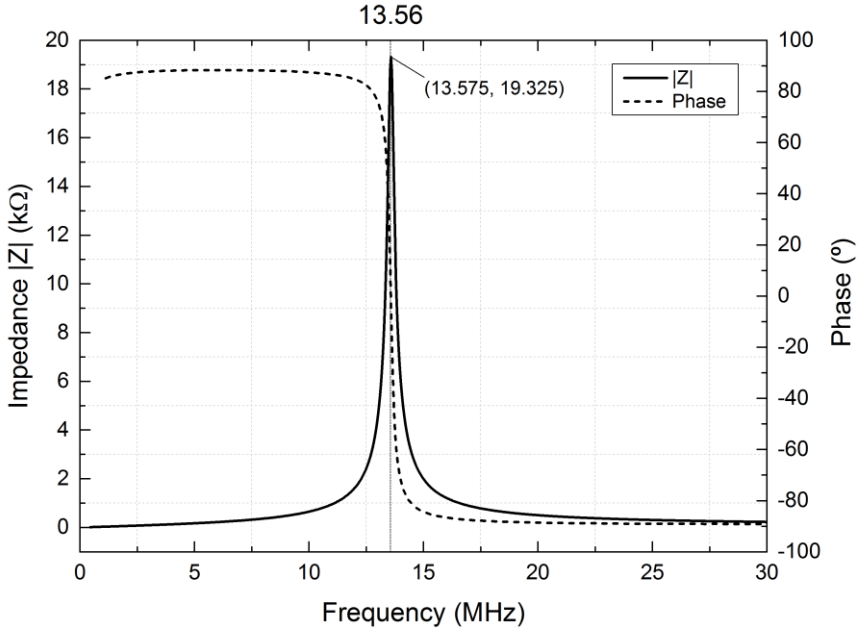

(b)

Figure 7. (a) Inductance and quality factor of PCB planar coil without the SL13A NFC chip. (b) Impedance and phase of the antenna coil with the SL13A chip soldered on the PCB.

5.2. Thermal dependence

The first step was to check the stability of the current source. The thermal dependence of the current source was measured using a 12 kΩ resistor (equivalent resistance of the ZVP3306 at 220 µA) as load and registering the current. The tag was supplied by a DC power source fixed at 6.4 V and it was placed into the climate chamber. The temperature was varied from 0 ºC to 50 ºC while the output current was measured. Applying a linear fitting, the thermal drift obtained was lower than 70 nA/ºC, which is good enough for our requirements. Therefore, we can consider the current source suitable for our design.

Once the thermal stability of the current source was verified, we studied the thermal dependence of the whole sensor module. Four sensor modules were placed into the climate chamber and the temperature was changed from 0 ºC to 50 ºC. The source voltage of the pMOS transistor, V_S, and the emitter voltage of the BJT, V_E, were registered (see Figure 3), and the thermal coefficient of these voltages were measured for each sensor module. Finally, the average thermal coefficients of the set of sensor modules was calculated. The global thermal coefficient of the set of sensor modules was reduced from (-1.80 ± 0.15) mV/ºC to (0.63 ± 0.10) mV/ºC. The thermal compensation was not as good as expected due to the difference between the thermal coefficient of the source voltage obtained in our previous work [34], (-2.30 ± 0.12) mV/ºC; and the thermal coefficient obtained in the present work (-1.80 ± 0.15) mV/ºC. Anyway the thermal coefficient reduction is enough for our requirements.

5.3. Dose measurements

To test the NFC reader unit, a comparison with our previously developed dose reader unit was carried out. Before irradiations, the source voltage for each sensor was measured with our previous reader and the developed NFC reader unit. Five minutes after the irradiation, the source voltage shift was measured. The obtained results from the three analysed sensors using both the NFC reader unit and the previous reader are displayed in Figure 8a and 8b, respectively, and summarised in Table 1 for the three studied sensors.

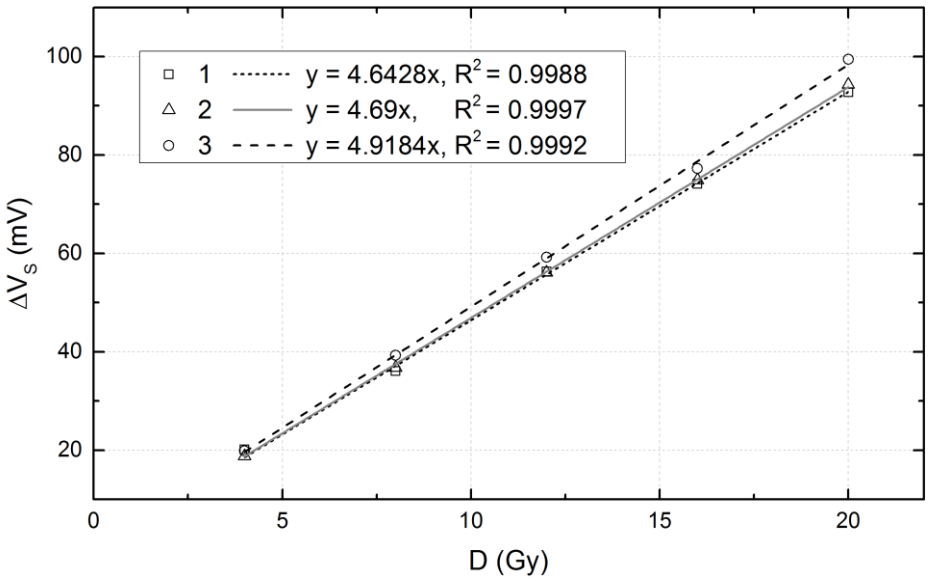

(a)

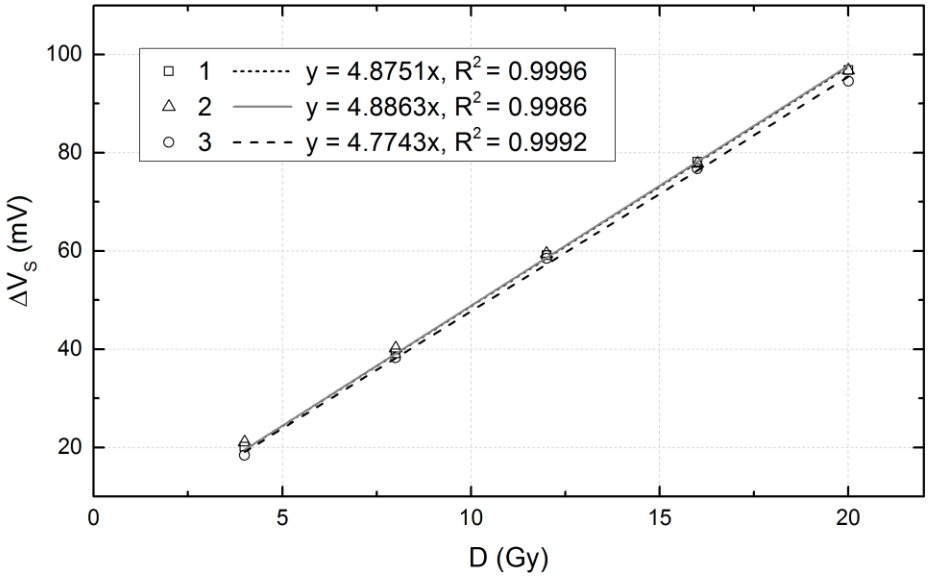

(b)

Figure 8. Accumulated source voltage shift versus dose measured by (a) the NFC reader unit; (b) the previously developed reader.

	#1	#2	#3	Average
NFC Reader	4.64 ± 0.03	4.69 ± 0.02	4.92 ± 0.03	**4.75 ± 0.15**
Previous Reader	4.88 ± 0.02	4.89 ± 0.04	4.77 ± 0.03	**4.85 ± 0.07**

Table 1. Sensitivities (mV/Gy) found for the three sensor modules using the NFC reader and the previous reader unit.

The average sensitivity found with the NFC reader unit is (4.75 ± 0.15) mV/Gy, which is in good agreement with the sensitivity measured by our previous reader, (4.85 ± 0.08) mV/Gy. As expected, a higher standard deviation is found with the NFC reader unit where the system simplicity does not allow the features of high performance readers. The value of the sensitivity found in the present work for the ZVP3306 is in agreement with previous studies [38]. The obtained sensitivity is approximately two times higher than the sensitivity achieved with Tyndall RADFETs of 100 nm oxide-gate thickness, but much lower than RADFETs of 400 and 1000 nm [39]. In any case, technical specifications of the presented architecture can be considered suitable to the majority of applications.

6. Conclusions

A dosimetric system based on a smartphone, an NFC tag and MOSFET dosimeters, developed using commercial integrated circuit, has been described and evaluated. The DMOS ZVP3306 has been used as dosimeter sensor. The main uncertainty source, the thermal drift, has been reduced using a bipolar buffer. To do so, the MOSFET and the bipolar transistors have been biased at appropriate drain and collector currents respectively, achieving a reduction of the thermal coefficient of 65 % in average. To carry out NFC measurements, a home-made structure made of wood was needed to ensure a good alignment between tag and smartphone antennas. Neglecting the current absorbed by the SL13A, the rest of NFC tag has a power consumption of 4 mW during the readout process, therefore a good inductive coupling must be achieved to carry out the measurements properly. The measurement process and the data storage were controlled by a custom-developed Android application. Finally, a dosimetric characterization was carried out using the NFC system and our reader unit presented in previous works, obtaining average sensitivities of (4.75 ± 0.15) mV/Gy and (4.85 ± 0.08) mV/Gy, respectively. Both values are in good agreement except for the uncertainty, which is higher for the NFC reader, but still acceptable for dose measurements. In both dosimetric systems a previous calibration would be required for accurate dose measurements.

Acknowledgements

The authors acknowledge the Servicio de Radiofísica (Radio-physics Service) of the Hospital Universitario San Cecilio (Granada, Spain) for permitting us to use their installations. This work was funded by the Spanish Government under project FPA2015-67694-P (Spanish Ministry of Economy, Industry and Competitiveness) and a R&D predoctoral grant (FPU13/05032, Spanish Ministry of Education, Culture and Sport). This project is partially supported by European Regional Development Funds (ERDF).

References

[1] R.C. Hughes, D. Huffman, J.V. Snelling, T.E. Zipperian, A.J. Ricco, C.A. Kelsey, Miniature radiation dosimeter for in vivo radiation measurements, Int. J. Radiat. Oncol. 14 (1988) 963–967. doi:10.1016/0360-3016(88)90019-3.

[2] M. Soubra, J. Cygler, G. Mackay, Evaluation of a dual bias dual metal oxide-silicon semiconductor field effect transistor detector as radiation dosimeter, Med. Phys. 21 (1994) 567–572. doi:10.1118/1.597314.

[3] G. Sarrabayrouse, S. Siskos, Radiation dose measurement using MOSFETs, IEEE Instrum. Meas. Mag. 1 (1998) 26–34. doi:10.1109/5289.685494.

[4] A.B. Rosenfeld, MOSFET dosimetry on modern radiation oncology modalities, Radiat. Prot. Dosimetry. 101 (2002) 393–398. http://www.ncbi.nlm.nih.gov/pubmed/12382775.

[5] I. Thomson, G.F. Mackay, M.P. Brown, Direct reading dosimeter, EP 0471957A3, 1991.

[6] A. Rozenfeld, Radiation sensor and Dosimeter (MOSkin), US 8,742,357 B2, 2008.

[7] S. Best, A. Ralston, N. Suchowerska, Clinical application of the OneDose^{TM} Patient Dosimetry System for total body irradiation, Phys. Med. Biol. 50 (2005) 5909–5919. doi:10.1088/0031-9155/50/24/010.

[8] N.D. Vasović, G.S. Ristić, A new microcontroller-based RADFET dosimeter reader, Radiat. Meas. 47 (2012) 272–276. doi:10.1016/j.radmeas.2012.01.017.

[9] M.A. Carvajal, F. Simancas, D. Guirado, M. Vilches, A.M. Lallena, A.J. Palma, A compact and low cost dosimetry system based on MOSFET for in vivo radiotherapy, Sensors Actuators A Phys. 182 (2012) 146–152. doi:10.1016/j.sna.2012.05.024.

[10] A. Holmes-Siedle, L. Adams, RADFET: A review of the use of metal-oxide-silicon devices as integrating dosimeters, Int. J. Radiat. Appl. Instrumentation. Part C. Radiat. Phys. Chem. 28 (1986) 235–244. doi:10.1016/1359-0197(86)90134-7.

[11] T.P. Ma, P. V. Dressendorfer, Ionizing radiation effects in MOS devices and circuits,

John Wiley & Sons, 1989.

[12] R.A. Price, C. Benson, M.J. Joyce, K. Rodgers, Development of a RadFET linear array for intracavitary in vivo dosimetry during external beam radiotherapy and brachytherapy, IEEE Trans. Nucl. Sci. 51 (2004) 1420–1426. doi:10.1109/TNS.2004.832570.

[13] E. Yilmaz, B. Kaleli, R. Turan, A systematic study on MOS type radiation sensors, Nucl. Instruments Methods Phys. Res. Sect. B Beam Interact. with Mater. Atoms. 264 (2007) 287–292. doi:10.1016/j.nimb.2007.08.081.

[14] M.S. Andjelković, G.S. Ristić, A.B. Jakšić, Using RADFET for the real-time measurement of gamma radiation dose rate, Meas. Sci. Technol. 26 (2015) 25004. doi:10.1088/0957-0233/26/2/025004.

[15] L.J. Asensio, M.A. Carvajal, J.A. L?pez-Villanueva, M. Vilches, A.M. Lallena, A.J. Palma, Evaluation of a low-cost commercial mosfet as radiation dosimeter, Sensors Actuators A Phys. 125 (2006) 288–295. doi:10.1016/j.sna.2005.08.020.

[16] M.S. Martínez-García, F. Simancas, A.J. Palma, A.M. Lallena, J. Banqueri, M.A. Carvajal, General purpose MOSFETs for the dosimetry of electron beams used in intra-operative radiotherapy, Sensors Actuators A. Phys. 210 (2014) 175–181. doi:10.1016/j.sna.2014.02.019.

[17] M. Carvajal, M. Martínez-García, D. Guirado, J. Banqueri, A. Palma, Dose verification system based on MOS transistor for real-time measurement, Sensors Actuators A. 247 (2016) 269–276. doi:10.1016/j.sna.2016.06.009.

[18] F. Li, Y. Bao, D. Wang, W. Wang, L. Niu, Smartphones for sensing, Sci. Bull. 61 (2016) 190–201. doi:10.1007/s11434-015-0954-1.

[19] V. Coskun, B. Ozdenizci, K. Ok, A Survey on Near Field Communication (NFC) Technology, Wirel. Pers. Commun. 71 (2013) 2259–2294. doi:10.1007/s11277-012-0935-5.

[20] P. Kassal, I.M. Steinberg, M.D. Steinberg, Wireless smart tag with potentiometric input for ultra low-power chemical sensing, Sensors Actuators B Chem. 184 (2013) 254–259. doi:10.1016/j.snb.2013.04.049.

[21] J. Fernandez-Salmeron, A. Rivadeneyra, M.A. Carvajal Rodriguez, L.F. Capitan-Vallvey, A.J. Palma, HF RFID Tag as Humidity Sensor: Two Different Approaches, IEEE Sens. J. 15 (2015) 5726–5733. doi:10.1109/JSEN.2015.2447031.

[22] H. Araki, J. Kim, S. Zhang, A. Banks, K.E. Crawford, X. Sheng, et al., Materials and Device Designs for an Epidermal UV Colorimetric Dosimeter with Near Field Communication Capabilities, Adv. Funct. Mater. 27 (2017) 1604465. doi:10.1002/adfm.201604465.

[23] A. Koh, D. Kang, Y. Xue, S. Lee, R.M. Pielak, J. Kim, et al., A soft, wearable microfluidic device for the capture, storage, and colorimetric sensing of sweat, Sci.

Transl. Med. 8 (2016). doi:10.1126/scitranslmed.aaf2593.

[24] J.M. Azzarelli, K.A. Mirica, J.B. Ravnsb?k, T.M. Swager, Wireless gas detection with a smartphone via rf communication, Proc. Natl. Acad. Sci. 111 (2014) 18162–18166. doi:10.1073/pnas.1415403111.

[25] D.P. Rose, M.E. Ratterman, D.K. Griffin, L. Hou, N. Kelley-Loughnane, R.R. Naik, et al., Adhesive RFID Sensor Patch for Monitoring of Sweat Electrolytes, IEEE Trans. Biomed. Eng. 62 (2015) 1457–1465. doi:10.1109/TBME.2014.2369991.

[26] P. Escobedo, M.M. Erenas, N. Lopez Ruiz, M.A. Carvajal, S. González Chocano, I. de Orbe-Payá, et al., Flexible Passive Nfc Tag for Multi-Gas Sensing, Anal. Chem. (2016) acs.analchem.6b03901. doi:10.1021/acs.analchem.6b03901.

[27] G. Xu, Q. Zhang, Y. Lu, L. Liu, D. Ji, S. Li, et al., Passive and wireless near field communication tag sensors for biochemical sensing with smartphone, Sensors Actuators, B Chem. 246 (2017) 748–755. doi:10.1016/j.snb.2017.02.149.

[28] P. Escobedo, M. Carvajal, L. Capitán-Vallvey, J. Fernández-Salmerón, A. Martínez-Olmos, A. Palma, Passive UHF RFID Tag for Multispectral Assessment, Sensors. 16 (2016) 1085. doi:10.3390/s16071085.

[29] R. Colella, L. Tarricone, L. Catarinucci, SPARTACUS: Self-Powered Augmented RFID Tag for Autonomous Computing and Ubiquitous Sensing, IEEE Trans. Antennas Propag. 63 (2015) 2272–2281. doi:10.1109/TAP.2015.2407908.

[30] J. Fernández-Salmerón, A. Rivadeneyra, F. Martínez-Martí, L. Capitán-Vallvey, A. Palma, M. Carvajal, Passive UHF RFID Tag with Multiple Sensing Capabilities, Sensors. 15 (2015) 26769–26782. doi:10.3390/s151026769.

[31] G.P. Beyer, G.G. Mann, J.A. Pursley, E.T. Espenhahn, C. Fraisse, D.J. Godfrey, et al., An Implantable MOSFET Dosimeter for the Measurement of Radiation Dose in Tissue During Cancer Therapy, IEEE Sens. J. 8 (2008) 38–51. doi:10.1109/JSEN.2007.912542.

[32] A.S. Beddar, M. Salehpour, T.M. Briere, H. Hamidian, M.T. Gillin, Preliminary evaluation of implantable MOSFET radiation dosimeters, Phys. Med. Biol. 50 (2005) 141–149. doi:10.1088/0031-9155/50/1/011.

[33] I. Buzurovic, T.N. Showalter, M.T. Studenski, R.B. Den, A.P. Dicker, J. Cao, et al., Commissioning and implementation of an implantable dosimeter for radiation therapy, J. Appl. Clin. Med. Phys. 14 (2013) 234–252. doi:10.1120/jacmp.v14i2.3989.

[34] M. Carvajal, M.S. Martínez-García, D. Guirado, A. Martínez-Olmos, A. Palma, Thermal compensation technique using the parasitic diode for DMOS transistors, Sensors Actuators A Phys. 249 (2016) 249–255. doi:10.1016/j.sna.2016.09.004.

[35] A. AG., SL13A: Smart Sensory Tag Chip For Unique Identification, Monitoring and Data Logging, 2014. http://ams.com/eng/Products/Wireless-Connectivity/Sensor-

Tags-Interfaces/SL13A.

[36] M.A. Carvajal, A. Martínez-Olmos, D.P. Morales, J.A. Lopez-Villanueva, A.M. Lallena, A.J. Palma, Thermal drift reduction with multiple bias current for MOSFET dosimeters, Phys. Med. Biol. 56 (2011) 3535–3550. doi:10.1088/0031-9155/56/12/006.

[37] M.A. Carvajal, M.S. Martínez-García, A. Martínez-Olmos, J. Banqueri, A.J. Palma, A simplified thermal model for lateral MOSFET and its application to temperature monitoring, Semicond. Sci. Technol. 29 (2014) 95017. doi:10.1088/0268-1242/29/9/095017.

[38] M.S. Martínez-García, J. Torres del Río, A. Jaksic, J. Banquerid, M.A. Carvajal, Response to ionizing radiation of different biased and stacked pMOSstructures, Sensors Actuators A Phys. 252 (2016) 67–75. doi: 10.1016/j.sna.2016.11.0070924-4247.

[39] E. Yilmaz, A. Kahraman, A.M. McGarrigle, N. Vasovic, D. Yegen, A. Jaksic, Investigation of RadFET response to X-ray and electron beams, Applied Radiation and Isotopes 127 (2017) 156-160. doi: 10.1016/j.apradiso.2017.06.004.